A modular platform for bioluminescent RNA tracking

Kevin K. Ng[†1], Kyle H. Cole[†2], Lila P. Halbers[†1], Claire Chen[1], Ahfnan A. Barhoosh[1], Edison Reid-McLaughlin[3], Mariajose Metcalfe[4], Alexandra D. Kent[3], Oswald Steward[*4], Andrej Lupták[*1–3], and Jennifer A. Prescher[*1–3]

[1]Department of Pharmaceutical Sciences, University of California, Irvine, Irvine, California 92697

[2]Department of Molecular Biology and Biochemistry, University of California, Irvine, Irvine, California 92697

[3]Department of Chemistry, University of California, Irvine, Irvine, California 92697

[4]Department of Anatomy and Neurobiology, University of California, Irvine, Irvine, California 92697

*Corresponding authors: (J.A.P.) Email: jpresche@uci.edu; (A.L.) Email: aluptak@uci.edu; (O.S.) Email: osteward@uci.edu

[†]These authors contributed equally

Abstract

Fluorescent probes have been used for decades to illuminate RNA dynamics in cells and transparent organisms. Serial imaging remains challenging, though, owing to toxicities associated with the required excitation light. Applications in live animals are also limited due to difficulties in delivering external light to target tissues. To circumvent these issues, we developed an alternative method for visualizing RNAs that relies on bioluminescence. Bioluminescence involves a chemical reaction between luciferase enzymes and luciferin small molecules that produces photons. Since no excitation light is required, bioluminescent probes do not exhibit phototoxicity or photobleaching effects. Additionally, little to no background signal is produced, providing high signal-to-noise ratios and enabling sensitive detection *in vivo* – an important consideration for visualizing low-copy transcripts. We engineered a unique RNA sequence that recruits bioluminescent molecules upon transcription. We further optimized this system to modularly tag and visualize RNAs in a variety of contexts. These results provide the foundation for visualizing RNA dynamics *in vivo*.

Introduction

RNA regulation underlies gene expression in all cell types ranging from germ cells[1–3] to immune cells[4] to neurons[5,6]. Understanding how RNA is dynamically regulated in response to specific cues and intracellular signaling pathways can shed light on the factors affecting complex cellular events, such as stem cell differentiation, immune function, and neuronal plasticity. To date, the fundamental blueprint of the RNA lifecycle, from transcription[7] and

processing[8] to polyadenylation[9,10], intracellular transport[11], subsequent translation, and degradation[12] has been established. However, little is known about the real-time dynamics of these events, particularly within the most physiologically relevant environment — live animals.

Our current understanding of RNA dynamics and localization derives primarily from *in vitro* and *in cellulo* analyses. Next generation sequencing technologies and modern structural biology techniques have provided detailed insights into RNA expression and structure. Additional information on RNA localization in cells has come from fluorescent *in situ* hybridization and other visualization techniques. While powerful, these methods all require RNA extraction for downstream analysis or fixed cells, precluding their application in dynamic experiments. This limitation has been partially addressed with the development of fluorogenic probes[13–17]. In particular, fluorescent proteins (FP) coupled with RNA binding proteins (RBP) such as the MS2 and PP7 bacteriophage coat proteins (MCP and PCP) have enabled live cell tracking of RNA in cell cultures and transparent organisms[18,19]. The FP-RBP fusion proteins bind target aptamers fused to transcripts of interest. Twelve or more aptamers are often required for reliable detection, though, resulting in very large protein-RNA complexes that can interfere with normal RNA dynamics. Moreover, these fluorescence-based methods are difficult to apply in living animals due to the need for excitation light delivery.

Bioluminescence is a complementary imaging technique that involves a chemical reaction between luciferase enzymes and luciferin small molecules to produce light[20,21]. Since no excitation light is required, there is virtually no background signal; thus, serial imaging is possible without concern for phototoxicity or tissue damage. Insect luciferases, such as firefly luciferase (FLuc), are routinely used in living animals to visualize cellular events such as cell movement and gene expression[22,23]. However, these probes tend to be dim, requiring large numbers for detectable signal. More recently reported engineered luciferases, such as NanoLuc, provide substantially higher photon outputs and improved thermal stability[24]. Red-shifted (and thus more tissue penetrant) light emission can be achieved by fusing NanoLuc to FPs[25–27]. We envisioned co-opting such bioluminescent proteins for RNA tagging via RBP attachment, similar to how FPs have been leveraged for live cell imaging. Direct fusions of luciferase to MS2/PP7 would result in probes that are always “on”, though, confounding downstream analyses. Both RNA-bound and unbound probes would produce light, and discriminating among them would be challenging given the sensitivity of bioluminescence imaging.

An alternative — and potentially more reliable — strategy for imaging RNA transcripts could leverage a “split” luciferase,[28,29] whereby fragments of the light-emitting enzyme produce photons only when bound to one another. One well known split luciferase, NanoBiT, features two engineered fragments (LgBiT and SmBiT) that are

non-functional until they bind and reassemble a functional NanoLuc enzyme[29]. NanoBiT complementation has been used extensively to examine protein-protein interactions and other biomolecular networks[21,30,31]. Background signal is diminished in the absence of the two pieces; robust photon output is observed only when both fragments are in proximity and capable of forming the heterodimer. The large turn-on resulting from NanoBiT assembly can enable more sensitive visualization of target localization and other biochemical events.

Herein, we report a bioluminescent platform that leverages split NanoLuc assembly to image RNA. NanoBiT was integrated with the MS2/PP7 system to enable sensitive detection of various transcripts. We extensively optimized the MS2 and PP7 RNA bait to provide maximal signal tun-on and minimize the size of the protein-RNA complex. The linkers fusing the MS2 coat protein (MCP) and PP7 coat protein (PCP) NanoBiT fragments were also optimized. We demonstrated the robustness of the RNA imaging platform *in vitro* and *in cellulo*. Additionally, we found that the novel MS2-PP7 RNA bait was modular and could be used in conjunction with other split luciferase enzymes. Collectively, these results set the stage for tracking RNA dynamics in live animals.

Results

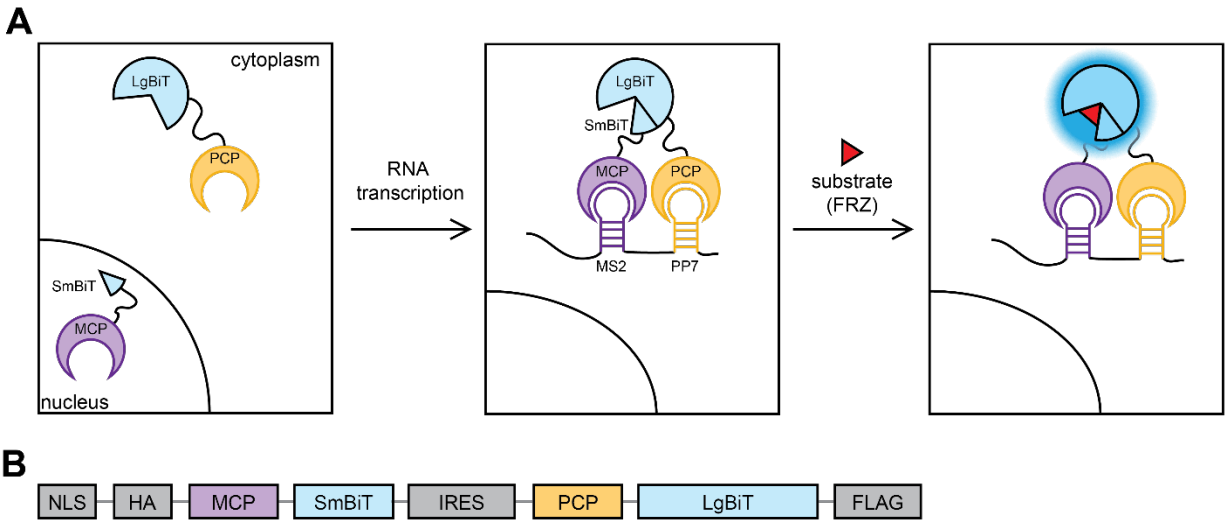

Figure 1. Platform to visualize and track RNA dynamics. A) Overall strategy to visualize RNA transcripts using MS2 coat protein (MCP) and PP7 coat protein (PCP) fused to NanoBiT fragments (SmBiT and LgBiT, respectively). Transcription of bait RNA (comprising MS2 and PP7 aptamers) drives NanoBiT heterodimerization. In the presence of a luciferin substrate (furimazine, FRZ), light is produced. B) Bicistronic construct encoding the luminescent RNA probe. MCP and PCP were fused with HA and FLAG tags, respectively, for expression analyses.

Our goal was to repurpose the MS2-PP7 system for luminescent tracing of RNA transcripts, building on NanoBiT, the well-known split luciferase reporter comprising a short peptide (SmBiT) and a larger protein fragment (LgBiT, **Fig. 1A**). Our approach involved appending each half of NanoBiT to either MCP or PCP. The resulting fusions would be capable of binding MS2-PP7 tagged RNA upon transcription, creating a functional luciferase enzyme. Luciferin addition would result in photon production, enabling visualization of transcript localization and, ideally, copy number measurement based on signal intensity. The overall strategy was dependent on three key steps: RNA bait transcription, MCP/PCP binding, and NanoBiT complementation and bioluminescence. Each step required optimization to achieve high photon output. We first designed an RNA bait that folded properly when tagged to a transcript of interest. We also required MCP and PCP fusion proteins that were properly localized and oriented upon RNA transcription. Finally, we had to ensure that LgBiT and SmBiT could be brought into proximity for efficient complementation upon MCP/PCP binding.

We designed a bicistronic construct using an internal ribosome entry site (IRES) to mediate co-expression of MCP and PCP (**Figure 1B**)[29,32]. MCP was fused to SmBiT, while PCP was fused to the larger protein fragment (LgBiT). This design differs from a previously published split-FP platform, in which MCP and PCP were fused to the N- and C-terminal fragments of the Venus fluorescent protein, respectively[18]. We modeled the fusion proteins using PyMOL to assess the feasibility of the design. No obvious steric clashes or unfavorable positioning with a 5′-MS2-PP7-3′ RNA bait were observed, indicating that NanoBiT assembly was possible under these conditions (**Supp Fig. 1**). The analyses further suggested that even a direct fusion of the MS2 and PP7 aptamers could support split luciferase complementation. Such a design would minimize the size of the bait and thus mitigate any disruption of the target RNA. Since the modeled assemblies were not energy minimized, we anticipated that additional engineering of the linkers and orientations would be necessary to maximize NanoBiT complementation upon MCP-PCP binding.

To further improve signal-to-noise ratios in the imaging output, MCP was tagged with a nuclear localization signal (NLS), whereas PCP was not tagged with NLS, to spatially separate MCP and PCP expression in the absence of the RNA bait. Confining the proteins to separate compartments would

reduce background complementation and thus enable more sensitive imaging. Expression of transcripts fused to the RNA bait would transit MCP from the nucleus into the cytoplasm (or capture *de novo* translated MCP in the cytoplasm). Cytoplasmic binding by PCP would then localize both halves of NanoBiT to the target transcript and enable reporter complementation.

The binding efficiency of NanoBiT can be tuned based on the SmBiT peptide sequence[29]. We examined two SmBiT peptides ($SmBiT^{high}$, K_D = 180 nM; $SmBiT^{low}$, K_D = 190 μM) to determine which would provide the best dynamic range: minimal signal in the absence of RNA bait and robust signal (due to high complementation efficiency) in the presence of RNA bait. Multimers of SmBiT were also evaluated in an attempt to enhance signal (**Supp. Fig2A**). The designer probes were first expressed using an *in vitro* transcription/translation system (IVTT) featuring T7 RNA polymerase transcription and rabbit reticulocyte lysate translation. Background signal was determined in the absence of RNA bait. Full complementation of translated NanoBiT was achieved via the addition of exogenous $SmBiT^{ultra}$ (K_D = 0.7 nM) or recombinant LgBiT at saturating concentrations, establishing the maximum potential signal (**Supp Fig2B**). All protein designs exhibited robust signal turn-on when $SmBiT^{ultra}$ or recombinant LgBiT was added, but high background signal was observed in the $SmBiT^{high}$ cases. Larger turn-ons were observed with $SmBiT^{low}$ designs (**Supp Fig 2C**). Additional copies of SmBiT did not yield signal enhancement, possibly due to steric interference from insufficient spacing between sequential peptides. Together, these data indicate that $SmBiT^{low}$ (hereby termed MP^{probe}) provides the highest dynamic range upon RNA complexation due to the low background complementation of the NanoBiT parts.

We next investigated whether MP^{probe} could bind the previously reported MS2-PP7 RNA bait (**Supp Fig. 3A**)[18]. An approximately 17-fold signal increase was observed with RNA bait transcription (via IVTT) in this case. The turn-on depended on the ratio of plasmid DNAs coding for RNA bait and MCP-SmBiT/PCP-LgBiT bicistronic mRNA (**Supp Fig. 3B**). The signal dependence on the RNA-to-protein ratio was attributed to the RNA bait structure. When the bait sequence was analyzed using Vienna RNAFold[33,34] and modeled in Forna[35], a flexible structure capable of sampling multiple conformations was observed (**Supp Fig. 3C**). While a flexible bait could aid NanoBiT complementation and thus signal turn-

on, too much movement could potentially interfere with heterodimerization. Such a platform would enable several non-productive conformations to be sampled, resulting in diminished signal-to-noise ratios.

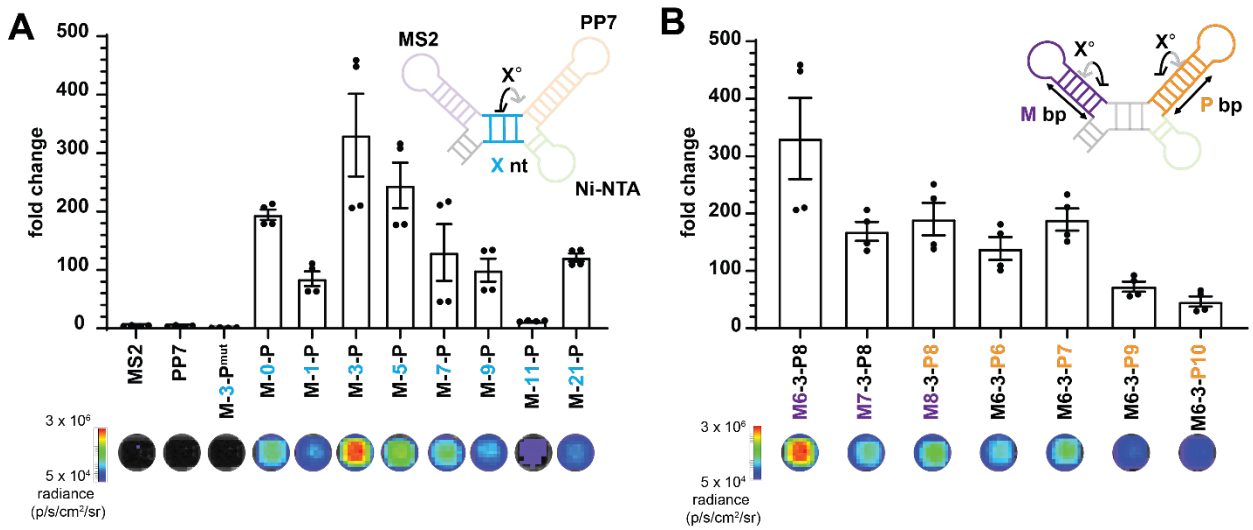

Figure 2. Engineered RNA bait provides robust photon output. A) RNA baits comprising varying spacers. The length of the spacer (X nt, blue, denoted below each bar graph) modulates the distance and phase angle between the MS2 and PP7 aptamers. RNA bait and MP^{probe} were produced using a T7 RNA polymerase and reticulocyte lysate IVTT system. Fold-change in signal over MP^{probe} alone is plotted. MS2, PP7, and M-3-P^{mut} denote baits comprising individual aptamers or a mutated PP7 aptamer, respectively, none of which were expected to result in complementation of MP^{probe}. Representative luminescence images are shown below the graph. B) RNA baits comprising various MS2 and PP7 stem lengths (top right, purple and orange for the MS2 and PP7 aptamers, respectively) were designed and tested. Following IVTT, luminescence readouts were acquired. The fold-change in signal over MP^{probe} alone is plotted. Representative luminescence images are shown below the graph. For (A)–(B), error bars represent the standard error of the mean (SEM) for n = 4 experiments.

We hypothesized that increasing the rigidity of the RNA bait would favor NanoBiT assembly and photon production. We thus sought to lock the spacing and orientation of the MS2 and PP7 aptamers. We redesigned the RNA bait by introducing an additional stem-loop structure, creating a 4-way junction. The stem-loop forms a Ni-NTA-binding aptamer[36]. We also sequentially increased the number of nucleotides within a spacer between the MS2 and PP7 aptamer domains (M-X-P, **Supp Fig. 4A**). In doing so, we sampled the phase angle up to ~180º and aptamer spacing up to ~3 nm. The redesigned RNA baits yielded significantly higher luminescence, with up to 334-fold increase over a no-RNA-bait control (**Figure 2A**). This signal increase remained highly dependent on the RNA bait to MP^{probe} DNA template ratio; however, the trends were consistent across the different baits examined (**Supp Fig. 4B**). Photon

production also depended on the RNA bait: in experiments using MS2, PP7, or MS2-PP7^{mut} RNA only (**Supp Fig. 5A**)[37], no appreciable signal over background was observed, regardless of the ratios of template DNAs (**Figure 2A, Supp Fig. 5B**).

Due to the improved luminescence achieved through modulating the distance and phase angle between the MS2 and PP7 aptamers, we attempted to optimize another parameter governing NanoBiT assembly: the relative length and rotation of the interacting aptamer faces relative to each other. To this end, we took the optimal M-3-P RNA bait and added base-pairs (bp) to either the MS2 or PP7 stem (**Supp Fig. 6A**). M-3-P comprises a 6-bp stem for MS2 and 8-bp for PP7. No additional improvements in light output were observed among this suite of probes, suggesting that the length and orientation of the two aptamers were already optimal (**Fig. 2B**). The results also indicated that aptamer stem lengths within two base pairs of each other were ideal. We confirmed that the lack of improvement was not a result of template DNA ratios (**Supp Fig. 6B**). Although the orientation of the aptamers had minimal effect on complementation, we found the positioning of the aptamers was critical. When MS2 was placed upstream of PP7, complementation was abrogated (**Supp Fig. 7A-B**). Of note, the optimized RNA bait design also supported the assembly of MCP and PCP fused to split fragments of firefly luciferase (**Supp Fig. 8A-C**), yielding a large increase in photon production.

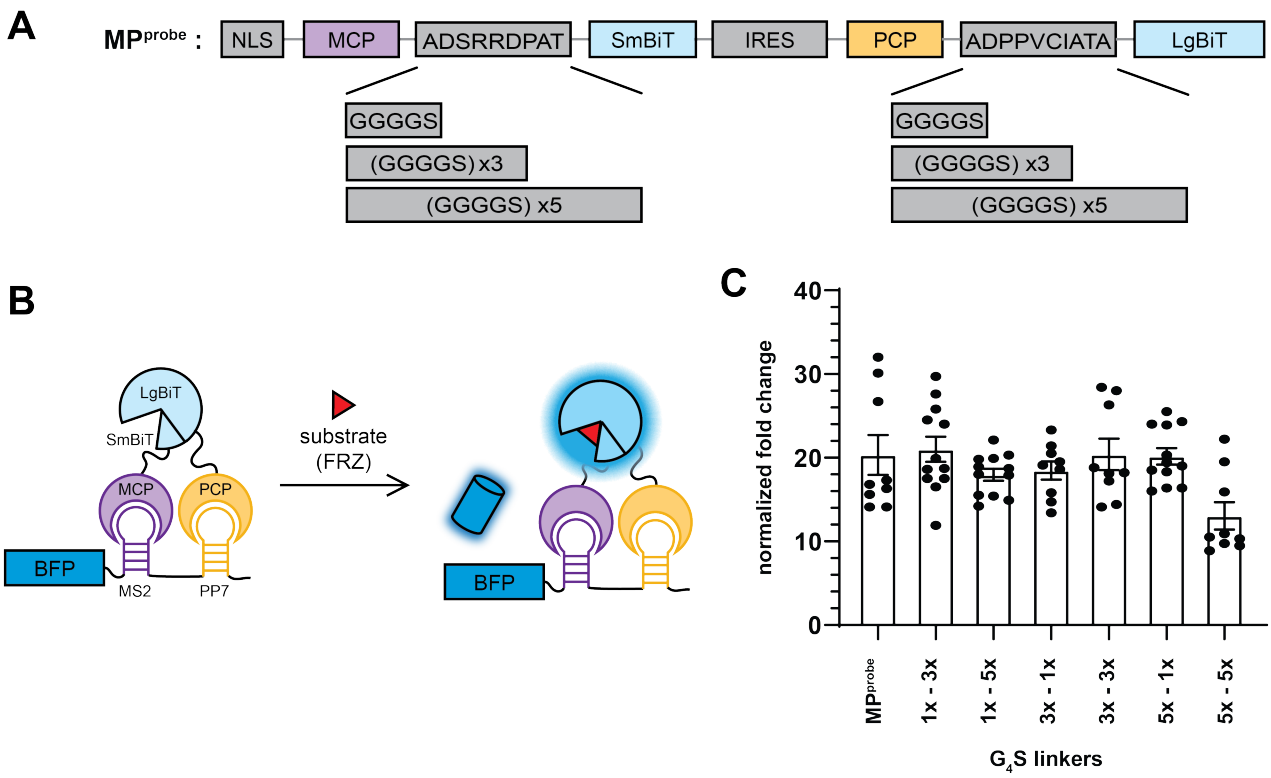

Figure 3. RNA imaging *in cellulo* with bioluminescent probes. A) MCP-PCP-NanoBiT fusions comprising various linker lengths were designed. All combinations of linkers were tested. B) BFP-encoding mRNA was used as a model transcript. The sequence was engineered with M-3-P in the 3′ UTR. Transcription of *BFP* mRNA enabled recruitment of the MCP-PCP-NanoBiT complex. BFP expression was confirmed by fluorescence. C) Luminescence measurements from cells stably expressing each linker design and transfected with the BFP-M-3-P construct. Data are plotted as the fold-change in signal over non-transfected cells and normalized for BFP expression. Nine replicates are shown, and the error bars represent the standard error of the mean (SEM) for all replicates.

Next, we investigated the effect of protein linker length on NanoBiT complementation. The initial protein linkers used in MP^{probe} were encoded through restriction enzyme cut-sites for cloning purposes and were potentially not optimal for luciferase assembly. Accordingly, we designed a suite of constructs containing up to five copies of a glycine-serine repeating unit (G_4S) between the RNA-binding proteins and the NanoBiT segments (**Figure 3A**). These constructs were then tested with the M-3-P, M-7-P, or M-11-P RNA baits using IVTT (**Supp Fig. 9A**). As with MP^{probe}, all novel linker combinations demonstrated the highest signal turn-on with the M-3-P RNA bait. Signal diminished somewhat with increasing distance and phase angle between MS2 and PP7. Interestingly, there was minimal (~1.5 fold) improvement in

signal turn-on with the modified glycine-serine linkers over the MP^{probe} design (**Supp Fig. 9B**). The data did suggest, though, that extremely long or short linkers were detrimental to NanoBiT complementation.

Having confirmed the robustness of MP^{probe} designs through IVTT, we characterized their applicability for imaging RNA *in cellulo*. We developed a model system using a BFP-encoding mRNA tagged with the M-3-P RNA bait in the 3′ UTR (**Figure 3B**). This platform enabled the verification of RNA bait production through BFP expression. Cells lines stably expressing various MCP and PCP fusions were generated and subsequently transfected with the M-3-P tagged BFP plasmid. Luminescence in transfected cells was normalized to BFP expression, as determined by flow cytometry. A ~20-fold increase in luminescence was observed in cells expressing M-3-P tagged transcripts (**Figure 3C**). Importantly, these *in cellulo* results mirrored the *in vitro* data, with minimal improvement over the starting MP^{probe} design observed with varying glycine-serine linkers. Perhaps most importantly, the 5x-5x design (five G_4S linkers in both protein fusions) exhibited reduced signal turn-on both *in vitro* and *in cellulo*, suggesting disfavored complementation with increasing linker length.

Discussion

We developed and optimized a novel luciferase-based platform to visualize RNA. This system combines the high signal-to-noise ratio of NanoBiT with the MS2-PP7 RBP systems to label transcripts tagged with an optimized MS2-PP7 RNA bait. We demonstrated a substantial improvement in signal turn-on with a rigid M-3-P design over the MS2-PP7 RNA bait used previously with split fluorescent proteins. Importantly, signal turn-on can be achieved using a single copy of M-3-P, as compared to 12 or more copies of previous MS2-PP7 aptamer designs. This design substantially decreases the size of the RNA-protein complex, reducing the likelihood of perturbations to RNA function and localization. Furthermore, M-3-P can be applied to other split luciferase systems. Our design only works when MS2 is located 5′ of PP7 and requires the binding of functional MS2 and PP7 aptamers on the same tagged transcript to localize and drive complementation of NanoBiT. This system is robust enough to function in the complex

environment of the cell; however, signal turn-on is likely dependent on the ratio of protein to target transcript.

Our platform provides a novel approach to visualizing and tracking transcripts, although certain aspects of the system remain to be fine-tuned. In particular, the ~300-fold turn-on from the M-3-P design observed *in vitro* was not replicated *in cellulo*. This was primarily due to the increased background signal *in cellulo*. Protein-to-transcript ratio is also a critical factor. Too much transcript relative to protein can create a “hook” effect, whereby MCP and PCP are recruited to different transcripts and prevent NanoBiT assembly. Conversely, low levels of target transcript may not co-localize enough MCP/PCP to drive sufficient signal production. Future studies will address these issues by tuning protein expression and validating transcript expression *in cellulo*.

This work sets the stage for tracking RNA dynamically in various settings ranging from *in vitro* to *in vivo*. The current work demonstrated visualization of a BFP transcript with the RNA bait incorporated into the 3′ UTR, however the short RNA bait tag can easily be applied to relevant transcripts through genetic manipulation. The modularity of our M-3-P design will enable the facile integration of other split luciferases or reporters for multiplexed RNA detection. Additionally, these designs can be combined with bioluminescent phasor analysis to quantify transcript levels at the single cell level over time. Together, these strategies that are built upon the reported work here will provide novel methods to visualize and quantify RNA without sacrificing the sample. In summary, our platform consisting of MCP-PCP-NanoBiT designer proteins and optimized M-3-P RNA bait provides a novel method to visualize RNA using luminescence.

Materials and Methods

General information

Q5 DNA polymerase, restriction enzymes, and all buffers were purchased from New England BioLabs. dNTPs were purchased from Thermo Fisher Scientific. Luria-Bertani medium (LB) was purchased from Genesee Scientific. All plasmids and primer stocks were stored at -20 °C unless otherwise noted. Primers were purchased from Integrated DNA Technologies and plasmids were sequenced by Genewiz. Sequencing traces were analyzed using Benchling.

General cloning methods

Polymerase chain reaction (PCR) was used to prepare genes of interest, and products were analyzed via gel electrophoresis. Products were excised and purified. Amplified genes were ligated into destination vectors via Gibson assembly[40]. All PCR reactions were performed in a BioRad C3000 Thermocycler using the following conditions: 1) 95 °C for 3 min, 2) 95 °C for 30 s, 3) –1.2°C per cycle starting at 72 °C for 30 s, 4) 72 °C for 30 sec, repeat steps 2–4 ten times, 5) 95 °C for 3 min, 6) 95 °C for 30 s, 7) 60 °C for 30 s, 8) 72 °C for 2 min repeat steps 6–8 twenty times, then 72 °C for 5 min, and hold at 12 °C until retrieval from the thermocycler. Gibson assembly conditions were: 50 °C for 60 min and hold at 12 °C until retrieval from the thermocycler. Ligated plasmids were transformed into TOP10 *E. coli* cells using the heat shock method. After incubation at 37 °C for 18–24 h, colonies were picked and expanded overnight in 5 mL LB broth supplemented with ampicillin (100 µg/mL) or kanamycin (100 µg/mL). DNA was extracted from colonies using a Zymo Research Plasmid Mini-prep Kit. DNA was subjected to restriction enzyme digest to confirm gene insertion. Positive hits were further sequenced.

General cell culture methods

HEK293T cells (HEK, ATCC) and stable cells lines derived from HEK293T cells were cultured in complete media: DMEM (Corning) containing 10% (v/v) fetal bovine serum (FBS, Life Technologies), penicillin (100 U/mL), and streptomycin (100 µg/mL, Gibco). Cell lines stably expressing MP^{probe} and linker designs were generated via lentiviral transduction. Transduced cells were further cultured with puromycin (20 µg/mL) to preserve gene incorporation. Cells were incubated at 37 °C in a 5% CO_2 humidified chamber. Cells were serially passaged using trypsin (0.25 % in HBSS, Gibco).

General flow cytometry methods

Cells were treated with trypsin for 5 min at 37 °C and then neutralized with complete media. Cells were transferred to Eppendorf tubes and pelleted (500 x*g*, 5 min) using a tabletop centrifuge (Thermo Fisher Sorvall Legend Micro 17). The resulting supernatants were discarded, and cells were washed with PBS (2×400 µL). Cells were analyzed for BFP expression on a Novocyte flow cytometer (ACEA BioSciences Inc). Live cells were gated and singlet cells were further gated. For each sample, 10,000 events were collected on the “singlet cell” gate.

IVIS imaging

All analyses were performed in black 384-well plates. Furimazine (20 µM, Promega) or D-luc (100 µM) and ATP (1 mM) were added to samples comprising NanoBiT or split firefly luciferase, respectively. Plates were imaged in a dark, light-proof chamber using an IVIS Lumina (PerkinElmer) CCD camera chilled to −90 °C. The stage was kept at 37 °C during imaging and the camera was controlled using Living Image software. Exposure times were set to 1 min and binning levels were set to medium. Regions of interest were selected for quantification and total flux values were analyzed using Living Image software. All data were exported to Microsoft Excel or PRISM (GraphPad) for further analysis.

Imaging on the iXon Ultra 888 EMCCD

Images were captured on an iXon Ultra 888 EMCCD (Oxford Instruments) equipped with a F 0.95 lens (Schneider) and imaged at a working distance of 30 cm on a black clear-bottom 384-well plate. Multiple images were captured with 5 sec exposures and 300 EM gain. Images were analyzed by stacking and Z projection in ImageJ. Densitometry was used to determine overall intensity for each well and the fold change in signal over no bait controls.

In vitro transcription/translation (IVTT) in rabbit reticulocyte lysate

A rabbit reticulocyte lysate *in vitro* translation kit (Promega, L4960) was coupled to *in vitro* transcription with the supplementation of $MgCl_2$, rNTPs, and T7 RNA polymerase. Plasmid DNAs were 3′ linearized for run-off transcription. RNA scaffolds were prepared via primer elongation of synthetic DNA oligos (Integrated DNA Technologies). Linearized plasmid DNAs and RNA bait DNAs were kit purified prior to IVTT (DNA Clean and Concentrator; Zymo Research, D4004). All DNAs were eluted into Tris-EDTA (TE; 10 mM Tris-HCl and 0.1 mM EDTA, pH 7.5) and controls were supplemented with an equal volume of TE buffer.

IVTT reactions were prepared on ice with 70% v/v lysate, 0.02 mM amino acid mix (-Leu/-Met), rNTPs (0.35 mM GTP and 0.15 mM each ATP/CTP/UTP), 1 mM $MgCl_2$, linearized plasmid DNA, RNA bait template DNA, 2 U/10 µL RNase inhibitor (Invitrogen, AM2694), and 0.5 µL/10 µL reaction of recombinant T7 RNA polymerase (house preparation). NanoBiT experiments were setup with 10 µL volumes and 1 nM of linearized plasmid DNA. Split firefly luciferase experiments were performed with 25 µL volumes and 3 nM of linearized plasmid DNA. RNA bait DNA templates were varied at specified ratios. IVTT reactions were incubated at 34 °C for 10 min and 30 °C for 140 min.

Luciferin substrates were supplied prior to imaging. For split NanoBiT experiments, furimazine was added to each reaction, and samples were incubated at room temperature for 5 min before imaging. For split firefly luciferase experiments, D-luciferin (100 µM) and ATP (1 mM) were added to each reaction. Samples were then incubated at room temperature for 5 min before image acquisition.

Protein expression and purification

LgBiT was encoded in a pCold vector. LgBiT was expressed in *E. coli* BL21 cells grown in LB medium (1 L). Expression was induced at an optical density (OD600) of ~0.6 by addition of 0.5 mM isopropyl-β-D-thiogalactopyranoside, followed by incubation at 37 °C for 4 h. Cells were harvested by centrifugation (4,000 x*g*, 10 min, 4 °C). Cells were then resuspended in lysis buffer (30 mL, 50 mM Tris HCl, 150 mM NaCl, 0.5% Tween-20, 1 mM phenylmethylsulfonyl fluoride, pH 7.4). Cells were sonicated (QSonica) at 40% amplitude, at 2 sec on 2 sec off intervals for 15 min. Cell debris was removed through centrifugation (10,000 x*g*, 1 h, 4 °C). Proteins were purified by Ni^{2+}-NTA affinity chromatography. Column was washed with wash buffer (20 mM imidazole, 50 mM $NaPO_4$, pH 7.4). Protein was eluted from column with elution buffer (200 mM Imidazole, 50 mM $NaPO_4$, pH 7.4). Protein was dialyzed overnight at 4 °C into phosphate buffer (50 mM $NaPO_4$, pH 7.4). Protein was concentrated to ~500 µL using Amicon Ultra-15 Centrifugal Filter Units (Merck Millipore MWCO 3 kDa). The concentration of proteins was determined using JASCO V730 UV-vis spectrophotometer at 280 nm. SDS-PAGE was also performed to verify purity, and gels were stained with Coomassie R-250.

In cellulo experiments

Stable cell lines of MP^{probe} or glycine-serine linker designs were plated in clear 12-well plates and incubated overnight. Cell lines were then transfected with using 1 µL Lipofectamine 3000, 2 µL P3000 Reagent, and 500 ng of the BFP-M-3-P plasmid. After 24 h incubation, cells were lifted and counted with a Countess II (Invitrogen). 50,000 transfected or non-transfected cells were plated in triplicate into black 96-well plates (Greiner Bio-One). Furimazine (20 µM) was added to each sample and imaged using an IVIS Lumina. Remaining cells were analyzed on a Novocyte flow cytometer for BFP expression.

References

1. Hake, L. E. & Richter, J. D. CPEB is a specificity factor that mediates cytoplasmic polyadenylation during Xenopus oocyte maturation. *Cell* **79**, 617–627 (1994).
2. Stebbins-Boaz, B., Hake, L. E. & Richter, J. D. CPEB controls the cytoplasmic polyadenylation of cyclin, Cdk2 and c-mos mRNAs and is necessary for oocyte maturation in Xenopus. *EMBO J.* **15**, 2582–2592 (1996).
3. Groisman, I. *et al.* CPEB, Maskin, and Cyclin B1 mRNA at the Mitotic Apparatus: Implications for Local Translational Control of Cell Division. *Cell* **103**, 435–447 (2000).
4. Karginov, T. A., Ménoret, A. & Vella, A. T. Optimal CD8+ T cell effector function requires costimulation-induced RNA-binding proteins that reprogram the transcript isoform landscape. *Nat. Commun.* **131**, 1–13 (2022).
5. Miyashiro, K., Dichter, M. & Eberwine, J. On the nature and differential distribution of mRNAs in hippocampal neurites: Implications for neuronal functioning. *Proc. Natl. Acad. Sci. U. S. A.* **91**, 10800–10804 (1994).
6. Farris, S., Lewandowski, G., Cox, C. D. & Steward, O. Selective Localization of Arc mRNA in Dendrites Involves Activity- and Translation-Dependent mRNA Degradation. *J. Neurosci.* **34**, 4481–4493 (2014).
7. Hobert, O. Gene regulation by transcription factors and MicroRNAs. *Science* **319**, 1785–1786 (2008).
8. Neugebauer, K. M. Nascent RNA and the Coordination of Splicing with Transcription. *Cold Spring Harb. Perspect. Biol.* **11**, a032227 (2019).
9. Ivshina, M., Lasko, P. & Richter, J. D. Cytoplasmic Polyadenylation Element Binding Proteins in Development, Health, and Disease. *Annu. Rev. Cell Dev. Biol* **30**, 393–415 (2014).
10. Movassat, M. *et al.* Coupling between alternative polyadenylation and alternative splicing is limited to terminal introns. *RNA Biol.* **13**, 646–655 (2016).
11. Shepard, P. J. *et al.* Complex and dynamic landscape of RNA polyadenylation revealed by PAS-Seq. *RNA* **17**, 761–772 (2011).
12. Łabno, A., Tomecki, R. & Dziembowski, A. Cytoplasmic RNA decay pathways - Enzymes and mechanisms. *Biochim. Biophys. Acta - Mol. Cell Res.* **1863**, 3125–3147 (2016).
13. Larson, D. R., Zenklusen, D., Wu, B., Chao, J. A. & Singer, R. H. Real-time observation of transcription initiation and elongation on an endogenous yeast gene. *Science* **332**, 475–478 (2011).
14. Halstead, J. M. *et al.* TRICK: A Single-Molecule Method for Imaging the First Round of Translation in Living Cells and Animals. *Methods Enzymol.* **572**, 123–157 (2016).
15. Song, W., Strack, R. L., Svensen, N. & Jaffrey, S. R. Plug-and-play fluorophores extend the spectral properties of spinach. *J. Am. Chem. Soc.* **136**, 1198–1201 (2014).
16. Steinmetzger, C., Palanisamy, N., Gore, K. R., & Höbartner, C. A Multicolor Large Stokes Shift Fluorogen-Activating RNA Aptamerw ith Cationic Chromophores. *Chem. Eur. J.* **25**, 1931–1935 (2019).
17. Dolgosheina, E. V *et al.* RNA Mango Aptamer-Fluorophore: A Bright, High-Affinity Complex for RNA Labeling and Tracking. (2014) doi:10.1021/cb500499x.
18. Wu, B., Chen, J. & Singer, R. H. Background free imaging of single mRNAs in live cells using split fluorescent proteins. *Sci. Reports* **41**, 1–3 (2014).
19. Campbell, P. D., Chao, J. A., Singer, R. H. & Marlow, F. L. Dynamic visualization of transcription and RNA subcellular localization in zebrafish. *Dev.* **142**, 1368–1374 (2015).
20. Love, A. C. & Prescher, J. A. Seeing (and Using) the Light: Recent Developments in Bioluminescence Technology. *Cell Chem. Biol.* **27**, 904–920 (2020).
21. Yeh, H.-W. & Ai, H.-W. Development and Applications of Bioluminescent and Chemiluminescent Reporters and Biosensors. *Annu. Rev. Anal. Chem.* **12**, 129–150 (2019).
22. Mezzanotte, L., van 't Root, M., Karatas, H., Goun, E. A. & Löwik, C. W. G. M. In Vivo Molecular Bioluminescence Imaging: New Tools and Applications. *Trends Biotechnol.* **35**, 640–652 (2017).
23. Syed, A. J. & Anderson, J. C. Applications of bioluminescence in biotechnology and beyond. *Chem. Soc. Rev.* **50**, 5668–5705 (2021).
24. Hall, M. P. *et al.* Engineered luciferase reporter from a deep sea shrimp utilizing a novel imidazopyrazinone substrate. *ACS Chem. Biol.* **7**, 1848–1857 (2012).
25. Suzuki, K. *et al.* Five colour variants of bright luminescent protein for real-time multicolour bioimaging. *Nat. Commun.* **7**, 13718 (2016).
26. Schaub, F. X. *et al.* Fluorophore-NanoLuc BRET reporters enable sensitive In Vivo optical imaging and flow cytometry for monitoring tumorigenesis. *Cancer Res.* **75**, 5023–5033 (2015).
27. Yeh, H. W. *et al.* ATP-Independent Bioluminescent Reporter Variants to Improve in Vivo Imaging. *ACS Chem. Biol.* **14**, 959–965 (2019).
28. Luker, K. E. *et al.* Kinetics of regulated protein-protein interactions revealed with firefly luciferase complementation imaging in cells and living animals. *Proc. Natl. Acad. Sci. U. S. A.* **101**, 12288–12293

(2004).
29. Dixon, A. S. *et al.* NanoLuc Complementation Reporter Optimized for Accurate Measurement of Protein Interactions in Cells. *ACS Chem. Biol.* **11**, 400–408 (2016).
30. Bodle, C. R., Hayes, M. P., O'Brien, J. B. & Roman, D. L. Development of a bimolecular luminescence complementation assay for RGS: G protein interactions in cells. *Anal. Biochem.* **522**, 10–17 (2017).
31. Machleidt, T. *et al.* NanoBRET—A Novel BRET Platform for the Analysis of Protein–Protein Interactions. *ACS Chem. Biol.* **10**, 1797–1804 (2015).
32. Mizuguchi, H., Xu, Z., Ishii-Watabe, A., Uchida, E. & Hayakawa, T. IRES-Dependent Second Gene Expression Is Significantly Lower Than Cap-Dependent First Gene Expression in a Bicistronic Vector. *Mol. Ther.* **1**, 376–382 (2000).
33. Gruber, A. R., Lorenz, R., Bernhart, S. H., Neuböck, R. & Hofacker, I. L. The Vienna RNA Websuite. *Nucleic Acids Res.* **36**, W70–W74 (2008).
34. Lorenz, R. *et al.* ViennaRNA Package 2.0. *Algorithms Mol. Biol.* **6**, 1–14 (2011).
35. Gendron, P., Lemieux, S. & Major, F. Quantitative analysis of nucleic acid three-dimensional structures. *J. Mol. Biol.* **308**, 919–936 (2001).
36. Chizzolini, F. *et al.* Large Phenotypic Enhancement of Structured Random RNA Pools. *J. Am. Chem. Soc.* **142**, 1941–1951 (2020).
37. Lim, F. & Peabody, D. S. RNA recognition site of PP7 coat protein. *Nucleic Acids Res.* **30**, 4138–4144 (2002).
38. Valegård, K. *et al.* The three-dimensional structures of two complexes between recombinant MS2 capsids and RNA operator fragments reveal sequence-specific protein-RNA interactions. *J. Mol. Biol.* **270**, 724–738 (1997).
39. Chao, J. A., Patskovsky, Y., Almo, S. C. & Singer, R. H. Structural basis for the coevolution of a viral RNA–protein complex. *Nat. Struct. Mol. Biol. 2008 151* **15**, 103–105 (2007).
40. Gibson, D. G. *et al.* Enzymatic assembly of DNA molecules up to several hundred kilobases. *Nat. Methods* **65**, 343–345 (2009).

Supplementary Figures

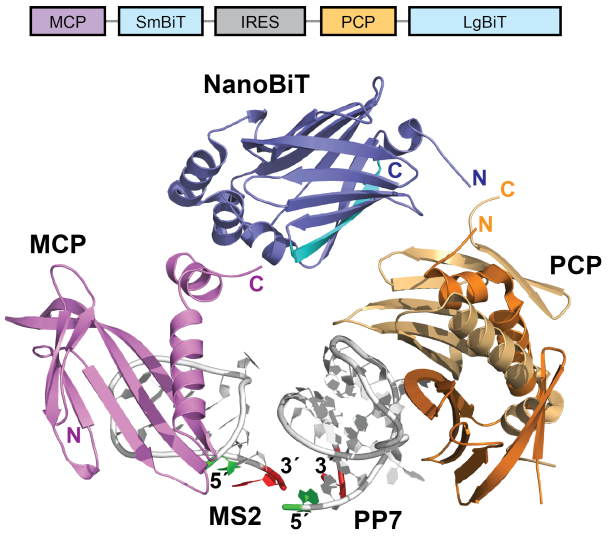

Supplementary Figure 1. Modeling of the MS2-PP7-NanoBiT complex. Crystal structures of MS2 (purple, 1ZDI)[38], PP7 (orange, 2QUX)[39] and NanoLuc (5IBO), highlighting LgBiT (dark blue) and SmBiT (cyan), were modeled in PyMOL. The MCP-SmBiT/PCP-LgBiT complex was modeled by aligning the corresponding N- and C- termini of each protein and aligning the 5' (green) and 3' (red) ends of the aptamers.

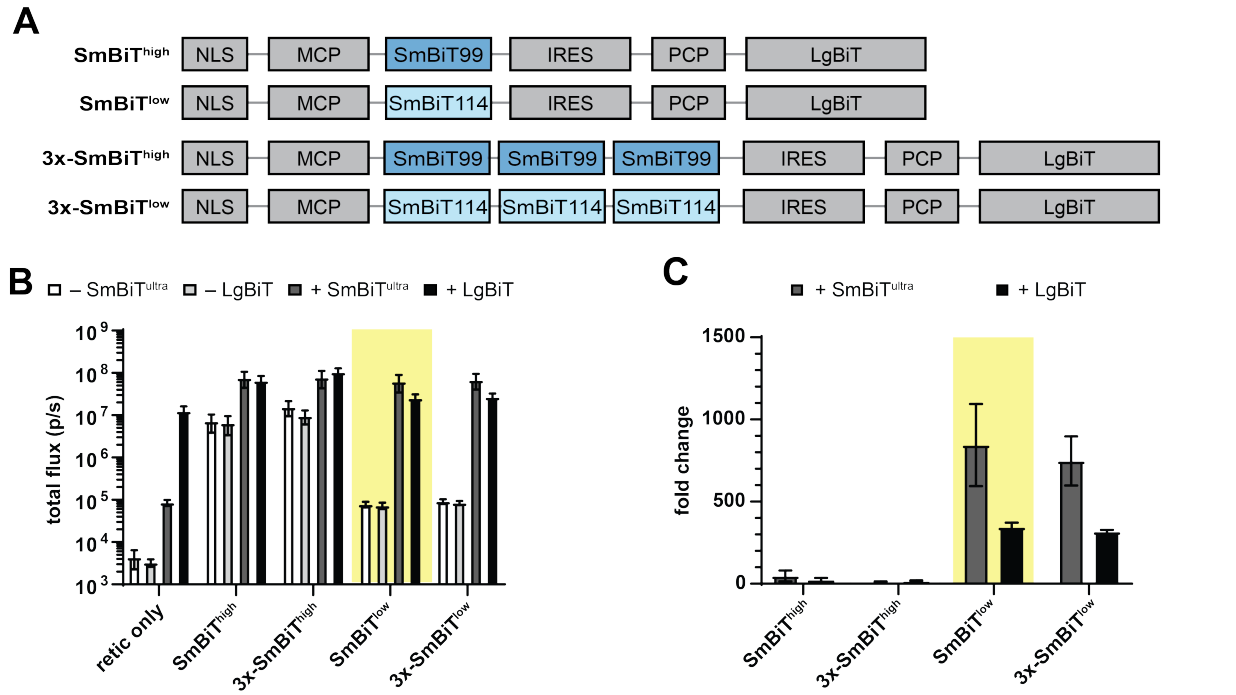

Supplementary Figure 2. Identifying the optimal SmBiT peptide. A) SmBiT99 (SmBiT^{high}) and SmBiT114 (SmBiT^{low}) were tested. Multimerization strategies were also examined with three sequential copies of SmBiT peptide. B) Luminescent probes were tested using IVTT. SmBiT86 (SmBiT^{ultra} ,10 μM) or recombinant LgBiT (10 μM) was added to samples and light outputs were measured. C) Fold change in light output (from B). For (B)-(C), error bars represent the standard error of the mean (SEM) for n = 3 replicates experiments.

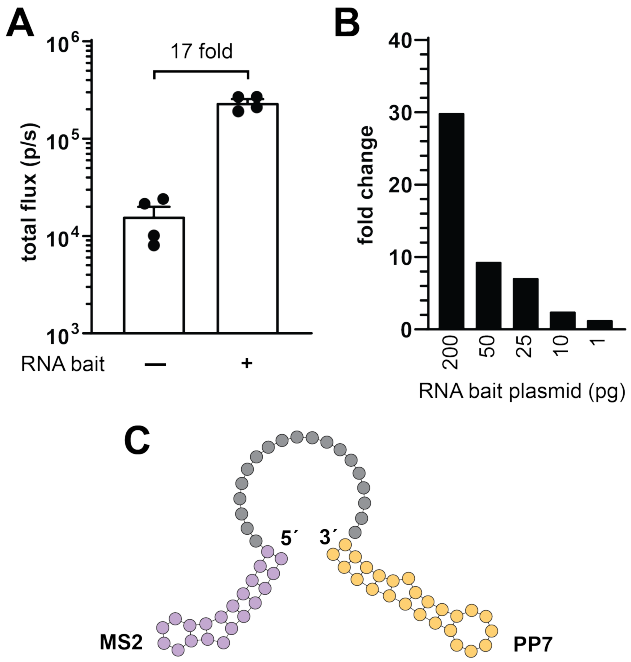

Supplementary Figure 3. Initial tests of luminescent probe with MCP/PCP RNA bait. A) Total flux observed in the absence or presence of RNA bait. B) Fold change in signal observed with varying ratios of RNA bait to probe DNA in an IVTT system. C) Structure of RNA bait as predicted by RNAfold and modeled in Forna. For (A)–(B), error bars represent the standard error of the mean (SEM) for n = 4 replicates.

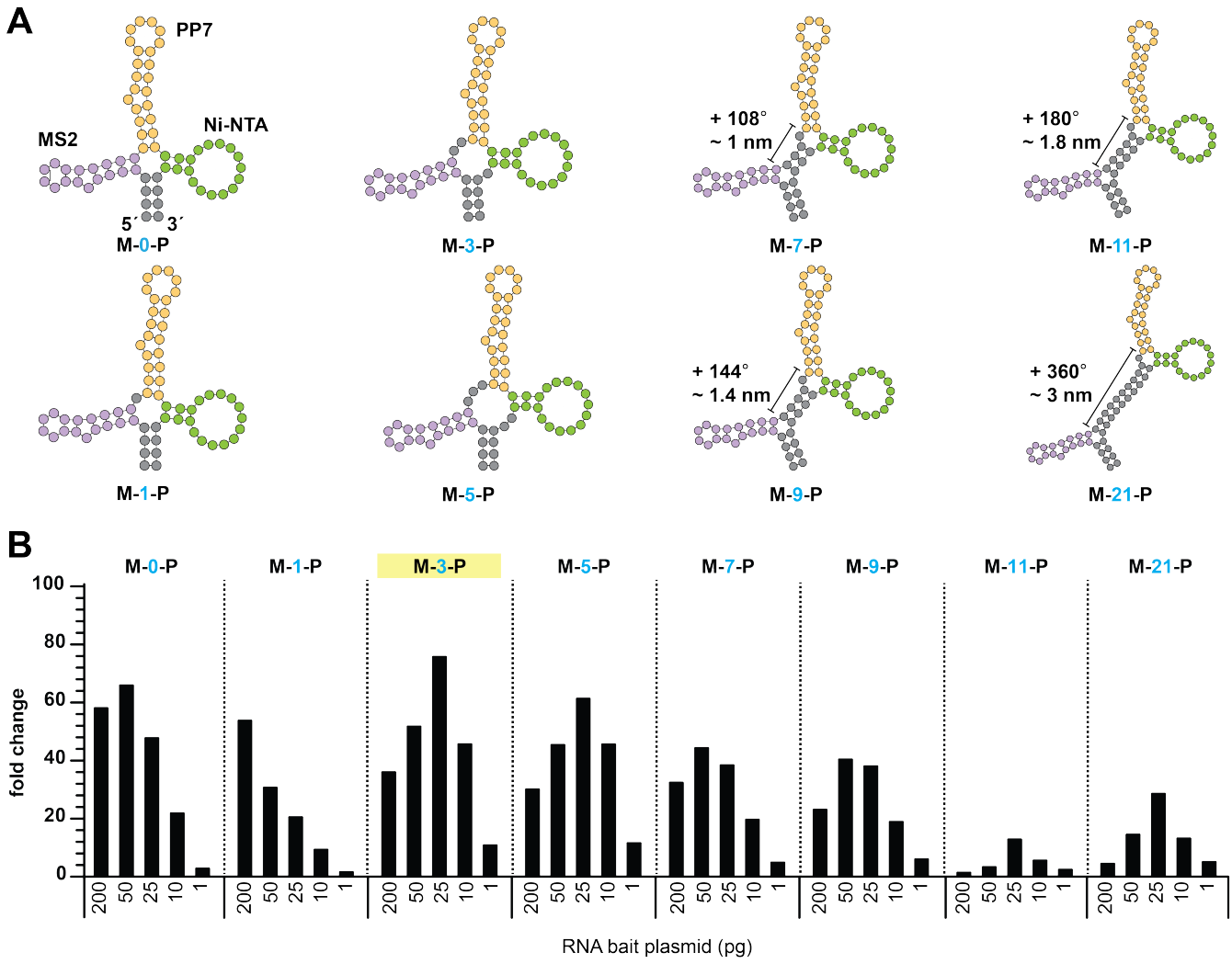

Supplementary Figure 4. Design of novel MCP/PCP RNA baits. A) RNA baits were redesigned, varying the number of nucleotides between the MS2 (purple) and PP7 (orange) aptamers. A Ni-NTA aptamer (green) was also added for purification purposes and improved structural rigidity. B) Luminescence readouts obtained with each RNA bait. Data are plotted as the fold change in signal from each RNA bait design over a no-RNA control sample. Decreasing concentrations of RNA bait template were tested with 1 ng of the probe (protein-coding) DNA plasmid. The mean fold change for each sample (n = 2) is shown.

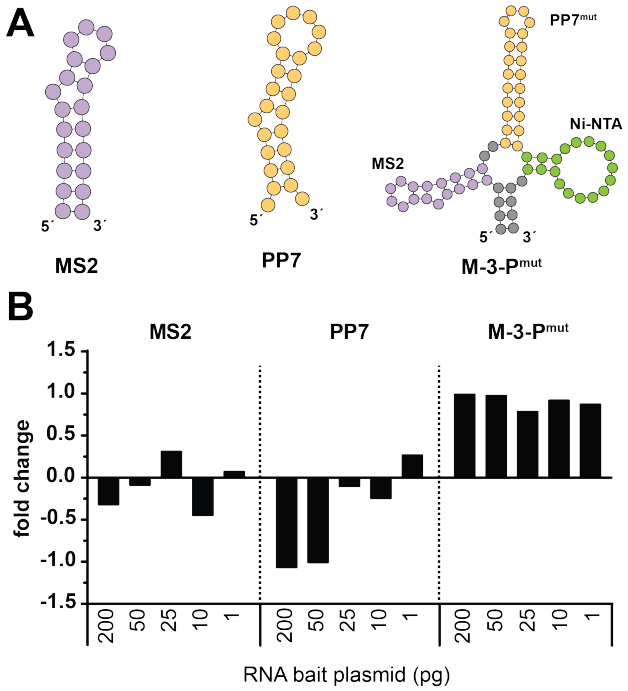

Supplementary Figure 5. No signal observed with control RNAs. A) Structures of control RNA baits were predicted using RNAfold and modeled in Forna. B) Fold change in signal observed with each control RNA bait design over a no-RNA sample. Decreasing concentrations of RNA bait template were tested with 1 ng of the probe DNA plasmid. The mean fold change for each sample (n = 2) is shown.

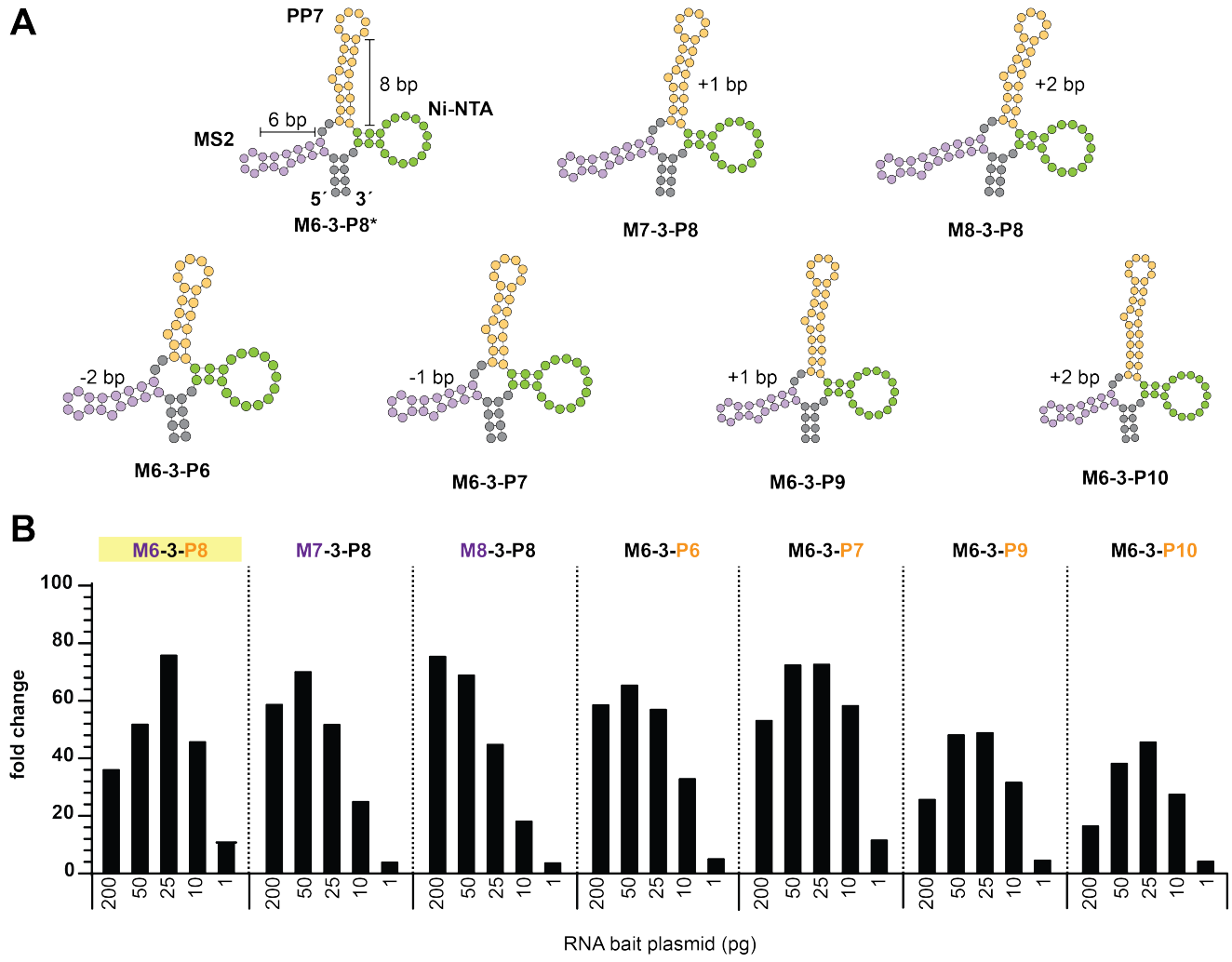

Supplementary Figure 6. Modulation of aptamer stem length. A) The stem regions of the MS2 (purple) and PP7 (orange) aptamers were modulated, varying the number of base pairs. Asterisk indicates RNA bait with unmodified MS2 and PP7 stems. B) Fold change in signal observed with each RNA bait design over a no-RNA control. Decreasing concentrations of each RNA bait template were tested with 1 ng of the probe DNA plasmid. The mean fold change for each sample (n = 2) is shown.

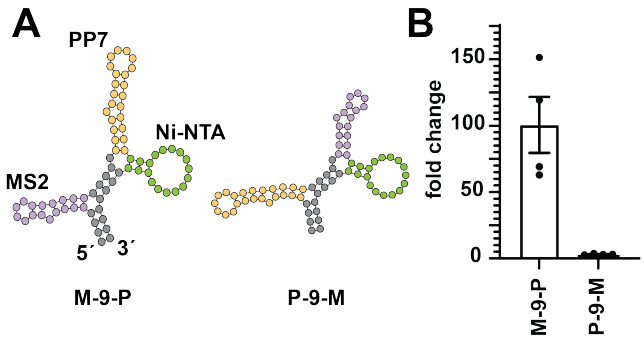

Supplementary Figure 7. Luminescent probe viable only with 5′-MS2–PP7-3′ configuration. A) The PP7 aptamer (orange) was placed 5′ of the MS2 aptamer (purple) to test the effect of binding site orientation on NanoBiT complementation. Predicted structures from RNAfold and modeled in Forna are shown for both orientations. B) RNA baits were tested using IVTT and the fold changes in light output over samples without RNA bait are plotted. Error bars represent the standard error of the mean (SEM) for n = 4 replicates.

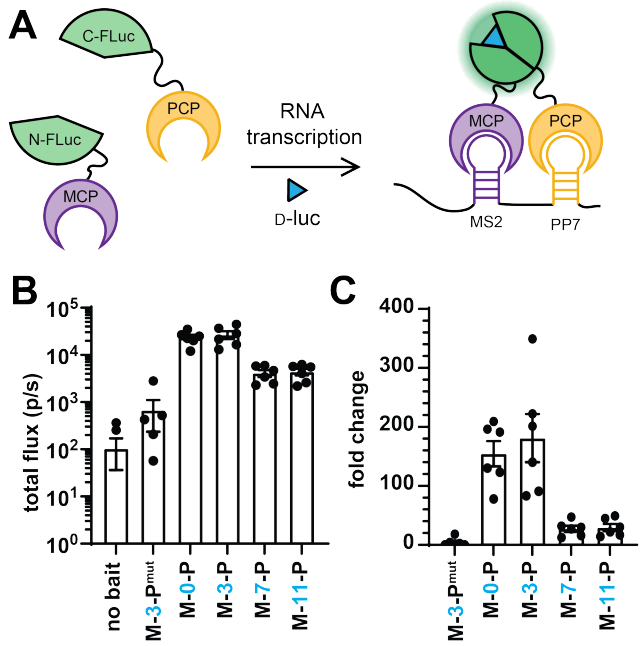

Supplementary Figure 8. RNA bait functions with other split reporters. A) Schematic of MCP/PCP probes fused to split FLuc. MCP is fused to the N-terminal half of FLuc and PCP is fused to the C-terminal half. RNA transcription followed by addition of D-luc enables photon production and visualization. B) The split-Fluc probe was tested against select RNA bait designs to sample their conformational landscape. Total light outputs for n = 6 replicates are shown. For the no-RNA bait sample, only 2 replicates are shown, as the others were below the limit of detection. C) Fold change in signal over no-RNA bait samples from B). For (B)–(C) error bars represent the standard error of the mean (SEM) for n = 6 replicates.

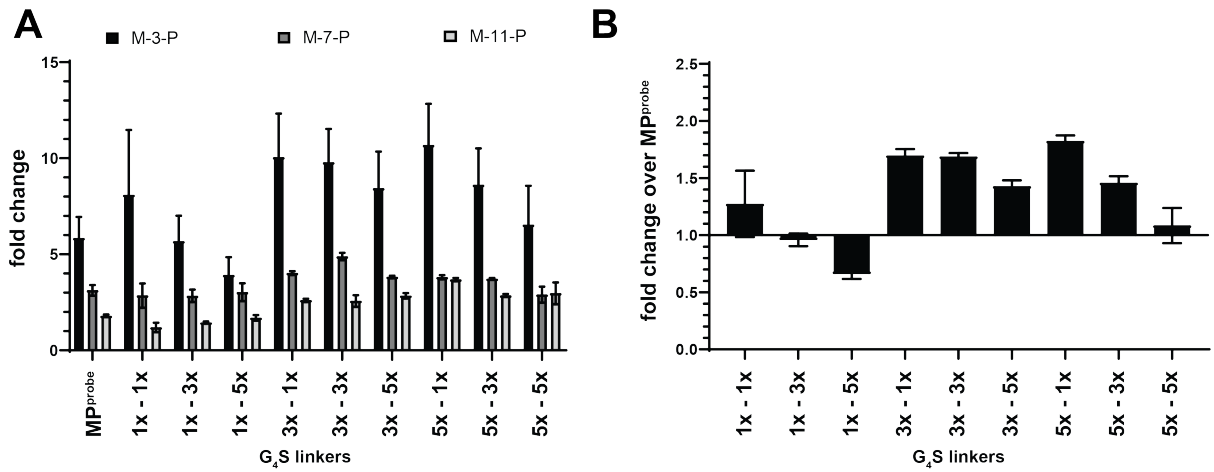

Supplementary Figure 9. Protein linker lengths have a smaller effect on photon output than RNA bait structure. A) Protein linkers comprising 1-5 copies of a glycine-serine repeating unit (G_4S) were examined. Luminescence outputs were recorded in the presence of various RNA baits. Data are plotted as the fold change in signal over no-RNA bait controls. B) Fold change in luminescence observed with probes comprising altered linkers and M-3-P versus MP^{probe} and M-3-P. No substantial increase in signal was observed with probes comprising G_4S units. For (A)–(B), error bars represent the standard error of the mean (SEM) for n = 4 replicates.